

How Does the Q_B Site Influence Propagate to the Q_A Site in Photosystem II?


Hiroshi Ishikita,^{*,†,‡} Koji Hasegawa,[§] and Takumi Noguchi^{||}

[†]202 Building E, Career-Path Promotion Unit for Young Life Scientists, Graduate School of Medicine, Kyoto University, Yoshida-Konoe-cho, Sakyo-ku, Kyoto 606-8501, Japan

[‡]Precursory Research for Embryonic Science and Technology (PRESTO), Japan Science and Technology Agency (JST), 4-1-8 Honcho, Kawaguchi, Saitama 332-0012, Japan

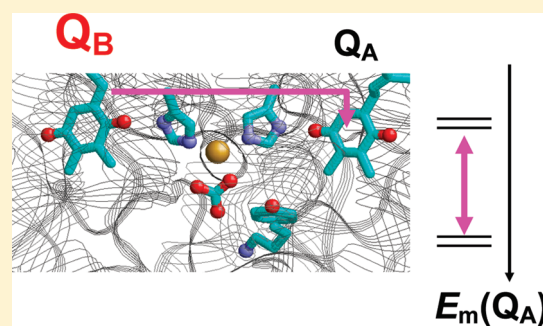
[§]AdvanceSoft Corporation, 1-9-20 Akasaka, Minato-ku, Tokyo 107-0052, Japan

^{||}Division of Material Science, Graduate School of Science, Nagoya University, Furo-cho, Chikusa-ku, Nagoya 464-8602, Japan

 Supporting Information

ABSTRACT: The redox potential of the primary quinone Q_A [$E_m(Q_A)$] in photosystem II (PSII) is lowered by replacement of the native plastoquinone (PQ) with bromoxynil (BR) at the secondary quinone Q_B binding site. Using the BR-bound PSII structure presented in the previous Fourier transform infrared and docking calculation studies, we calculated $E_m(Q_A)$ considering both the protein environment in atomic detail and the protonation pattern of the titratable residues. The calculated $E_m(Q_A)$ shift in response to the replacement of PQ with deprotonated BR at the Q_B binding site [$\Delta E_m(Q_A)_{PQ \rightarrow BR}$] was -55 mV when the three regions, Q_A , the non-heme iron complex, and Q_B ($Q_B = PQ$ or BR), were treated as a conjugated supramolecule (Q_A-Fe-Q_B). The negative charge of BR apparently contributes to the downshift in $\Delta E_m(Q_A)_{PQ \rightarrow BR}$.

This downshift, however, is mostly offset by the influence of the residues near Q_B . The charge delocalization over the Q_A-Fe-Q_B complex and the resulting H-bond strength change between Q_A and D2-His214 are crucial factors that yield a $\Delta E_m(Q_A)_{PQ \rightarrow BR}$ of -55 mV by (i) altering the electrostatic influence of the H-bond donor D2-His214 on $E_m(Q_A)$ and (ii) suppressing the proton uptake events of the titratable residues that could otherwise upshift $\Delta E_m(Q_A)_{PQ \rightarrow BR}$ during replacement of PQ with BR at the Q_B site.



The photosynthetic reaction in photosystem II (PSII) is initialized by light absorption. Beginning with a charge separation process at accessory chlorophyll Chl_{D1} , the resulting electronic excitation energy is ultimately converted to chemical potential.^{1–3} The charge separation forms an oxidized, positively charged $P680^+$, while the released electron travels along the electron transfer chain. The electron transfer is terminated by two plastoquinones (PQ), Q_A and Q_B , at the stromal side (reviewed in ref 4). The non-heme Fe complex is equidistant from both Q_A and Q_B . Two His residues, D1-His215 and D2-His214, are the ligands of the non-heme Fe complex that form an H-bond with Q_B and Q_A , respectively (Figure 1). These cofactors are located in the vicinity of the hydrophilic loops that connect the transmembrane helix D with helix *de* (D–*de* loop) parallel to the membrane plane in the D1 and D2 proteins. The D–*de* loop in PSII is rich in titratable and polar residues. The corresponding loop is absent in the bacterial photosynthetic reaction centers (reviewed in ref 5).

The original quinone, i.e., PQ at the Q_B binding site, is often subjected to replacement by herbicides. Consequently, the transfer of electrons from Q_A to Q_B is impaired. Additionally, it is widely known that herbicide binding at the Q_B site alters the

redox potential of Q_A for one-electron reduction [$E_m(Q_A)$]. The binding of phenolic herbicides at the Q_B site downshifts $E_m(Q_A)$ by ~ 45 mV, whereas urea-type herbicides [e.g., 3-(3,4-dichlorophenyl)-1,1-dimethylurea (DCMU)] upshift $E_m(Q_A)$ by ~ 50 mV.⁶

The shift in the $E_m(Q_A)$ value appears to be a key factor in determining the charge recombination pathway for the $P680^+Q_A^-$ state. As discussed in ref 7 in the O_2 -evolving PSII, charge recombination of $P680^+Q_A^-$ seems to occur via $P680^+Pheo_{D1}^-$. If the $E_m(Q_A)$ value is upshifted (the high-potential Q_A form) relative to the value in the original O_2 -evolving PSII, the corresponding charge recombination process could occur directly, not via $P680^+Pheo_{D1}^-$, because the E_m difference between Q_A and $Pheo_{D1}$ is sufficiently large.⁷ The $P680^+Pheo_{D1}^-$ state is known to generate triplet states at Chl_{D1} in high yield, leading to the harmful singlet oxygen. Thus, it has been proposed that the high-potential Q_A form plays a photo-protective role because charge recombination of $P680^+Q_A^-$ occurs without involving the triplet-generating $P680^+Pheo_{D1}^-$.

Received: December 21, 2010

Revised: May 16, 2011

Published: May 17, 2011

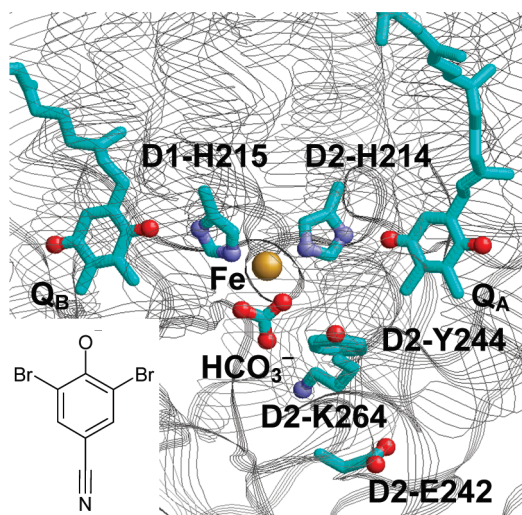


Figure 1. Residues in the neighborhood of the non-heme Fe in PSII. Carbon, nitrogen, and oxygen atoms are colored cyan, blue, and red, respectively. The chemical structure of deprotonated bromoxynil that can be replaced with Q_B is also shown.

state.^{7,8} The existence of two competing pathways for charge recombination of the $P680^+Q_A^-$ state, originally proposed for bacterial photosynthetic reaction centers,^{9,10} is supported by mutational studies varying the pheophytin redox potential.¹¹

The $E_m(Q_A)$ shift caused by herbicide binding at the Q_B site should play a role in photoprotection of PSII. However, the detailed mechanism of how the Q_B binding site can control $E_m(Q_A)$ remains unclear, partly because the crystal structure of herbicide-bound PSII is unknown. On the other hand, FTIR studies have provided structural information related, in particular, to H-bonds between quinones and the H-bond partners. Takano et al.¹² showed that the H-bonding interaction of Q_A is altered by binding of different types of herbicides at the Q_B site. Takahashi et al.¹³ also reported that D1-His215, which donates an H-bond to Q_B in the native PSII, forms an H-bond with the phenolate oxygen of the deprotonated BR (Figure 1) in BR-bound PSII and presented the structural models of herbicide binding in the Q_B pocket based on the FTIR results and docking calculations. The latter authors concluded that the strength of the H-bond between D2-His214 and Q_A is affected by the interaction between D1-His215 and an herbicide at the Q_B site through the Q_A –His–Fe–His–herbicide bridge. To answer the essential question of how the $E_m(Q_A)$ level is controlled by the Q_B side, which is ~ 13 Å from Q_A , we calculated $E_m(Q_A)$ using the herbicide-bound PSII structures that were put forward on the basis of their FTIR results¹³ and considered the protonation states of all titratable sites in the entire PSII.

COMPUTATIONAL PROCEDURES

Coordinates. The initial atomic coordinates of PSII were taken from the X-ray structure of the PSII complexes from *Thermosynechococcus elongatus* at 2.9 Å resolution [Protein Data Bank (PDB) entry 3BZ2¹⁴]. The PQ- and BR-bound PSII structures in which PQ-1 and deprotonated BR were situated at the Q_B binding site, respectively, were obtained as described in the previous study.¹³ The initial PQ-9-bound structure was geometry optimized by molecular mechanics (MM) calculation with the XUFF force field¹⁵ using ABINIT-MP,¹⁶ and the poses

of PQ-1 and BR in the Q_B pocket were determined by docking calculation using AutoDock.¹⁷ For the BR-bound PSII structure, partial geometry optimization by MM calculation was further performed for the Q_B pocket, including BR, the non-heme iron, its four histidine ligands (D1-His215, D1-His272, D2-His214, and D2-His268), and Met214, Leu218, Val219, Tyr246, Ile248, Ala251, His252, Phe255, Ser264, Phe265, and Leu271 (see the Supporting Information for the atomic coordinates of the modeled region). For error estimates, see ref 15.

Note that BR is most likely to be present in deprotonated form at the Q_B binding site.¹³ There is experimental evidence of the deprotonated form of BR in the Q_B pocket. (i) The frequencies of the CN (~ 2209 cm^{-1}) and CO (1516 cm^{-1}) stretching vibrations of BR in the Q_B pocket, which were obtained by FTIR measurements of Q_A^-/Q_A^{12} and $\text{Fe}^{2+}/\text{Fe}^{3+}$ differences,¹³ were much closer to those of the deprotonated form than those of the protonated form measured in an ethanol solution. (ii) The $\text{Fe}^{2+}/\text{Fe}^{3+}$ FTIR difference spectra of PSII in the presence of BR showed a strong H-bond interaction of D1-His215, which is consistent with a strong H-bond formation of this His with the deprotonated CO group of BR.¹³ As for additional theoretical evidence of deprotonated BR, docking calculation predicted a direct H-bond interaction between D1-His215 and BR when BR has a deprotonated form, whereas neutral BR was predicted to bind to the opposite side of the pocket without a specific interaction with D1-His 215.¹³

Using the obtained PQ- and BR-bound PSII structures, hydrogen atoms were generated and energetically optimized with CHARMM,¹⁸ while the positions of all non-hydrogen atoms were fixed and all titratable groups kept in their standard protonation states; i.e., acidic groups were ionized, and basic groups (including titratable His residues) were protonated. Simultaneously, chlorophylls, pheophytins, and quinones were kept in a neutral charge state, and the non-heme Fe was kept in the reduced state, Fe^{2+} . His residues that are ligands of the non-heme Fe and chlorophylls were treated as nontitratable with neutral total charge.

Atomic Partial Charges. Atomic partial charges of the amino acids were adopted from the all-atom CHARMM22¹⁹ parameter set. The charges of the protonated acidic O atoms were increased symmetrically by 0.5 unit charges to account implicitly for the presence of a proton. Similarly, instead of the removal of a proton in the deprotonated state, the charges of all the protons of the basic groups of Arg and Lys were diminished symmetrically by a total unit charge. For residues whose protonation states were not available in the CHARMM22 parameter set, appropriate charges were computed.²⁰ For the cofactors (e.g., the MnCa cluster, chlorophylls, pheophytins, and quinones), the same atomic charges as in previous computations of PSII^{5,8,21} were used. The atomic charges of (i) the high-spin non-heme Fe (that is, comprised of one Fe ion, one bicarbonate, and D1-His215, D2-His214, D1-His272, and D2-His268) and (ii) the non-heme Fe, Q_A , and Q_B complexes (Q_A –Fe– Q_B where Q_B is PQ or BR) were determined from the electronic wave functions by fitting the resulting electrostatic potential in the neighborhood of these molecules using the RESP procedure²² (Table S1 of the Supporting Information). The electronic wave functions were calculated after geometry optimization with the DFT module in JAGUAR²³ using the B3LYP functional with the LACVP* basis set (6-31G* with effective core potentials on heavy atoms).

Computation of E_m . The typical computational conditions and procedures used in the previous studies on the non-heme

Fe complex⁵ and quinones⁸ were consistently used in this study. This computation is based on the electrostatic continuum model by solving the linear Poisson–Boltzmann (LPB) equation with the MEAD program.²⁴ To facilitate a direct comparison with previous computational results, identical computational conditions and parameters were used (e.g., refs 5, 8, and 21) such as atomic partial charges and dielectric constants. The redox states of all other cofactors (e.g., chlorophylls, pheophytins, and quinones) were kept in their neutral charge state during redox titration of Q_A . The ensemble of the protonation patterns was sampled by the Monte Carlo method with Karlsberg²⁵ (B. Rabenstein, Karlsberg online manual, <http://agknapp.chemie.fu-berlin.de/karlsberg/>, 1999). For the first 3000 MC scans, random protonation changes were applied for all individual titratable residues. For the remaining 7000 MC scans, titratable residues whose protonation probability deviated by less than 10^{-6} from zero or unity were fixed at the corresponding pure protonation state.

The dielectric constants were set as follows: $\epsilon_p = 4$ inside the protein, and $\epsilon_w = 80$ for water. All computations were performed at 300 K, pH 7.0, and an ionic strength of 100 mM. The LPB equation was solved using a three-step grid-focusing procedure at resolutions 2.5, 1.0, and 0.3 Å. The Monte Carlo sampling for a redox active group yielded the probabilities $[A_{ox}]$ and $[A_{red}]$ of the two redox states of molecule A. The E_m was evaluated from the Nernst equation. A bias potential was applied to obtain an equal amount of both redox states ($[A_{ox}] = [A_{red}]$), yielding the redox midpoint potential E_m as the resulting bias potential. For the sake of convenience, the computed E_m was given with millivolt accuracy, without implying that the last digit is significant.

In general, values of E_m ranging over a few millivolts fall within a sufficiently reproducible range for our computational method. Systematic errors typically relate to specific conformations that may differ from the given crystal structures. In particular, the difference between the H-bond patterns among conformations is crucial: the presence or absence of an H-bond at the focusing site is responsible for a value shift of 60–100 mV in E_m for quinones.^{8,26} Similar results were also reported by other groups.²⁷ (Note that errors of >100 mV most likely originate from changes in the atomic coordinates, and this is not the case for our computations because of the fixation of the heavy-atom position in the crystal structures.)

To generate appropriate H-bonds in the proteins, the consideration of the protonation states of the titratable residues is very important.^{8,26} To minimize the uncertainty in the generated atomic coordinates because of the limitation of the empirical force field parametrization, we made frequent use of fixed atomic coordinates during titration after optimizing all the hydrogen atomic coordinates with the relevant protonation states by using a procedure similar to that used in ref 20. We believe that the atom positions at which the crystallographers observed the corresponding electron density should be evaluated with the highest priority. Although the atomic coordinates of the original crystal structures are not optimized in terms of the bond length or angles, most crucial is the H-bonding pattern for the energetics of the focusing region. We used the model structures for the PQ- and BR-bound PSII¹³ in this study. Thus, we paid specific attention to the atomic coordinates of the model structures that might be involved in the H-bond. A direct H-bond between D1-His215 and BR was observed in the deprotonated BR-bound PSII model structure, which is in agreement with the presence of a strong H-bond observed from the FTIR measurements of Q_A^-/Q_A ¹² and Fe^{2+}/Fe^{3+} .¹³ In contrast, a neutral BR was

predicted to bind to the opposite side of the pocket without a specific interaction with D1-His215.¹³ Hence, the modeled structure should be used for computations only when the validity of the structure is confirmed by additional information (e.g., experimental results).

Influence of the Protein Dielectric Constant ϵ_p and pH on E_m . We used an ϵ_p of 4 only for the space covered by the merged van der Waals volumes of protein atoms. The Q_B binding site is apparently highly exposed to the bulk solvent. The $\Delta E_m(Q_A)_{PQ \rightarrow BR}$ values $\{=[E_m(Q_A) \text{ in BR-bound PSII}] - [E_m(Q_A) \text{ in PQ-bound PSII}]\}$ are calculated to be -55 mV [$\epsilon_p = 4$ (see below for the conditions)], -52 mV ($\epsilon_p = 6$), and -52 mV ($\epsilon_p = 8$). In this study, we consider the protonation states of all the titratable sites in the entire protein explicitly, i.e., the flexibility of the protein charge when all the titratable sites are simultaneously equilibrated; most other computational studies do not consider this flexibility. It is important to note that the protonation pattern is modulated in response to the Q_A redox state. Thus, the influence of the change in the ϵ_p value on E_m is partly offset by the modulation of the protonation states of all the titratable sites.

The Q_A –Fe– Q_B region of PSII is very close to the D–*de* loop that is rich in titratable and polar residues. Protein conformations in the loop region may be altered in response to the bulk pH value because of changes in the protonation states of the titratable residues. To eliminate this uncertainty, we fixed the atomic coordinates of the protein structure and evaluated the $\Delta E_m(Q_A)_{PQ \rightarrow BR}$ value only at a single pH value (7.0). Note that, using the fixed atomic coordinates, we calculated the $\Delta E_m(Q_A)_{PQ \rightarrow BR}$ values to be -57 mV at pH 6.0, -55 mV at pH 7.0, and -58 mV at pH 8.0 in this study.

RESULTS AND DISCUSSION

Induced $E_m(Q_A)$ Shift upon BR Binding. The $\Delta E_m(Q_A)_{PQ \rightarrow BR}$ value $\{=[E_m(Q_A) \text{ in BR-bound PSII}] - [E_m(Q_A) \text{ in PQ-bound PSII}]\}$ is calculated to be -55 mV using the atomic partial charges calculated for the conjugated Q_A –Fe– Q_B system ($Q_B = PQ$ or BR). The calculated $\Delta E_m(Q_A)_{PQ \rightarrow BR}$ is considerably close to the experimentally measured value of approximately -45 mV.⁶ By contrast, the $\Delta E_m(Q_A)_{PQ \rightarrow BR}$ value is calculated to be -13 mV, using the atomic partial charges calculated separately for Q_A , Fe, and Q_B ($Q_B = PQ$ or BR) molecules (nonconjugated Q_A /Fe/ Q_B system).

Although the net charges of the conjugated and nonconjugated systems are identical, charge distributions over the Q_A , Fe (including four His ligands and one bicarbonate ligand), and Q_B regions are considerably different in the two systems: $[Q_A]^0/[Fe]^+/[PQ]^0$ and $[Q_A]^0/[Fe]^+/[BR]^{-1}$ for the nonconjugated systems and $[Q_A]^{0.09}-[Fe]^{0.82}-[PQ]^{0.09}$ and $[Q_A]^{0.09}-[Fe]^{0.67}-[BR]^{-0.76}$ for the conjugated systems (Table S1 of the Supporting Information). In the Q_A –Fe–BR system, negative charges that originate from the BR region are partially moved to the Fe region. Thus, the Fe region, i.e., the direct H-bond partner of Q_A in the Q_A –Fe–BR system, is more negatively charged than in the Q_A /Fe/BR system. The more negatively charged Fe region in the Q_A –Fe–BR system destabilizes the anionic Q_A^- state and, as a result, downshifts $\Delta E_m(Q_A)_{PQ \rightarrow BR}$ exclusively in the Q_A –Fe– Q_B system.

This result demonstrates that the experimentally measured value of -45 mV⁶ can be reproduced only when we consider the quinones and the non-heme Fe as a single supramolecule and

Table 1. Influence of Protein Components on $E_m(Q_A)$ in PQ- and BR-Bound PSII in Millivolts^a

group	$Q_A\text{--Fe--}Q_B$				$Q_A/\text{Fe}/Q_B$			
	PQ	BR	$\Delta E_m(Q_A)_{PQ\rightarrow BR}$		PQ	BR	$\Delta E_m(Q_A)_{PQ\rightarrow BR}$	
	influence on $E_m(Q_A)$				influence on $E_m(Q_A)$			
(a) Key Protein Components Downshifting $E_m(Q_A)$ in BR-Bound PSII (relative to PQ-bound PSII)								
Q_B site	2	−40	−42	$(Q_B)^b$	−2	−49	−47	$(Q_B)^b$
D2-His214	146	105	−41	$(\text{Fe})^c$	186	166	−20	$(\text{Fe})^c$
D1-His215	17	8	−9	$(\text{Fe})^c$	28	27	−1	$(\text{Fe})^c$
D1-Tyr246	6	3	−3	$(\text{Fe})^c$	6	3	−3	$(\text{Fe})^c$
total			−95				−71	
(b) Key Protein Components Upshifting $E_m(Q_A)$ in BR-Bound PSII (relative to PQ-bound PSII).								
D2-Tyr244	−20	−8	12	$(\text{Fe})^e$	−64	−11	53	$(\text{Fe})^e$
D2-Lys264	127	138	11	$(\text{Fe})^e$	122	136	14	$(\text{Fe})^e$
D2-Glu242	−39	−34	5	$(\text{Fe})^e$	−29	−40	−11	$(\text{Fe})^e$
D2-His268	32	37	5	$(\text{Fe})^e$	34	44	10	$(\text{Fe})^e$
D2-Arg139 ^d	19	23	4	$(\text{else})^f$	19	23	4	$(\text{else})^f$
Fe	119	122	3	$(\text{Fe})^e$	115	114	−1	$(\text{Fe})^e$
total			40				69	

^a Protein components that increase or decrease $\Delta E_m(Q_A)$ by ≥ 3 mV are listed. For the sake of clarity, other residues have been omitted. ^b Molecule location: Q_B binding site. ^c Molecule location: ligands or neighbors of the non-heme Fe. ^d $N\eta_{D2\text{--}Arg139}\text{--}N\eta_{CP47\text{--}Arg7}$ distance of 5.8 Å. ^e Molecule location: ligands or neighbors of the non-heme Fe. ^f Molecule location: others.

implies the importance of the network that proceeds from Q_B to Q_A via the non-heme Fe. This is in line with outcomes from FTIR studies in which the H-bond strength between D1-His215 and Q_B could alter the H-bond strength in the Q_A side and shift $\Delta E_m(Q_A)_{PQ\rightarrow BR}$.^{12,13} Similar control modes (the H-bond network between Q_A and Q_B via Fe) have been reported for the bacterial photosynthetic reaction centers.^{28–33}

Protein Components That Decrease $\Delta E_m(Q_A)$. Despite the identical net charge for the $Q_A\text{--Fe--}Q_B$ and $Q_A/\text{Fe}/Q_B$ systems, the resulting $\Delta E_m(Q_A)_{PQ\rightarrow BR}$ values are significantly different. In all systems (irrespective of PQ or BR), the following groups commonly contribute to the significant $E_m(Q_A)$ downshifts: bicarbonate (133–138 mV), D1-Glu244 (73 mV), D2-Glu219 (61 mV), CP43-Glu464 (41 mV), and D2-Met246 (39 mV). Because these groups commonly decrease the $E_m(Q_A)$ values in all of the systems, they are not responsible for the difference in the resulting $\Delta E_m(Q_A)_{PQ\rightarrow BR}$ values for the $Q_A\text{--Fe--}Q_B$ and $Q_A/\text{Fe}/Q_B$ systems. To understand the detailed mechanism of differentiating the $\Delta E_m(Q_A)_{PQ\rightarrow BR}$ values for the $Q_A\text{--Fe--}Q_B$ and $Q_A/\text{Fe}/Q_B$ systems, we investigated the contributions of protein components to $\Delta E_m(Q_A)_{PQ\rightarrow BR}$. It appears that BR and D2-His214 are major components that downshift $\Delta E_m(Q_A)_{PQ\rightarrow BR}$ (Table 1a).

BR. In the $Q_A\text{--Fe--}Q_B$ system, BR downshifts $\Delta E_m(Q_A)_{PQ\rightarrow BR}$ by 42 mV (Table 1a). Interestingly, BR also contributes to a similar magnitude of the $\Delta E_m(Q_A)_{PQ\rightarrow BR}$ downshift in the $Q_A/\text{Fe}/Q_B$ system [$\Delta E_m(Q_A)_{PQ\rightarrow BR} = -47$ mV], indicating that the electrostatic influence of the negatively charged BR on $\Delta E_m(Q_A)_{PQ\rightarrow BR}$ is essentially the same in both conjugated and nonconjugated systems and is not responsible for the calculated $\Delta E_m(Q_A)_{PQ\rightarrow BR}$ difference in the two systems (Table 1a).

D2-His214, Which Donates an H-Bond to Q_A . One of the non-heme Fe ligands, D2-His214, provides an H-bond to the Q_A carbonyl group and could stabilize the Q_A reduced anionic state.

In the $Q_A/\text{Fe}/Q_B$ nonconjugated system, the influence of D2-His214 on $\Delta E_m(Q_A)_{PQ\rightarrow BR}$ is slightly weaker for BR-bound PSII than for PQ-bound PSII, resulting in a $\Delta E_m(Q_A)_{PQ\rightarrow BR}$ of −20 mV (Table 1a). The $\Delta E_m(Q_A)_{PQ\rightarrow BR}$ downshift by D2-His214 is mainly due to the larger H-bond distance between Q_A and D2-His214 in BR-bound PSII ($O_{QA}\text{--}N\delta_{His}$ distance of 3.0 Å) than that in PQ-bound PSII ($O_{QA}\text{--}N\delta_{His}$ distance of 2.8 Å). A larger H-bond distance leads to a weaker H-bond strength and results in a weaker Q_A^- state stabilization. In the $Q_A\text{--Fe--}Q_B$ system, however, the influence of D1-His214 on $\Delta E_m(Q_A)_{PQ\rightarrow BR}$ is 2 times greater (−41 mV). Because we used the same PSII model structures for both the conjugated and nonconjugated systems, the difference in the influence of D1-His214 on $\Delta E_m(Q_A)_{PQ\rightarrow BR}$ (−41 and −20 mV, respectively) can be attributed solely to the difference in the atomic partial charges for the conjugated and nonconjugated systems.

Thus, it can be concluded that the entire $\Delta E_m(Q_A)_{PQ\rightarrow BR}$ of −41 mV in the $Q_A\text{--Fe--}Q_B$ system is comprised of −20 mV due to the structural change induced by BR binding [i.e., the D1-His214 contribution to $\Delta E_m(Q_A)_{PQ\rightarrow BR}$ in the $Q_A/\text{Fe}/Q_B$ system, as shown in Table 1a] and the remaining −21 mV due to the induced change in the charge distribution over the $Q_A\text{--Fe--}Q_B$ system, i.e., the conjugation effect (Figure 2). Thus, the conjugation effect is a key factor in allowing the $Q_A\text{--Fe--}Q_B$ system [$\Delta E_m(Q_A)_{PQ\rightarrow BR} = -55$ mV] to reproduce the experimentally observed $\Delta E_m(Q_A)_{PQ\rightarrow BR}$ value,⁶ by also inducing the H-bond strength change between D1-His214 and Q_A .

Protein Components That Diminish the $\Delta E_m(Q_A)$ Downshift. In the $Q_A/\text{Fe}/Q_B$ system, the $\Delta E_m(Q_A)_{PQ\rightarrow BR}$ downshift of −71 mV by BR, D2-His214, D1-His214, and D1-Tyr246 (Table 1a) is finally offset by the influence of protein components D2-Tyr244, D2-Lys264, D2-Glu242, D2-His268, and D2-Arg139 and the Fe atom. In turn, these groups contribute to the $\Delta E_m(Q_A)_{PQ\rightarrow BR}$ upshift of 69 mV (Table 1b), almost completely compensating for the downshift. However, in the $Q_A\text{--Fe--}Q_B$

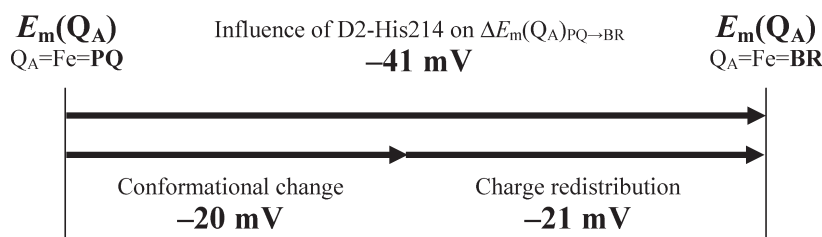


Figure 2. Influence of D2-His214 on $\Delta E_m(Q_A)_{PQ \rightarrow BR}$ in the Q_A –Fe– Q_B system. Note that this influence is independent of the influence of the proton uptake of the titratable residues on $\Delta E_m(Q_A)_{PQ \rightarrow BR}$; i.e., the two influences are additive.

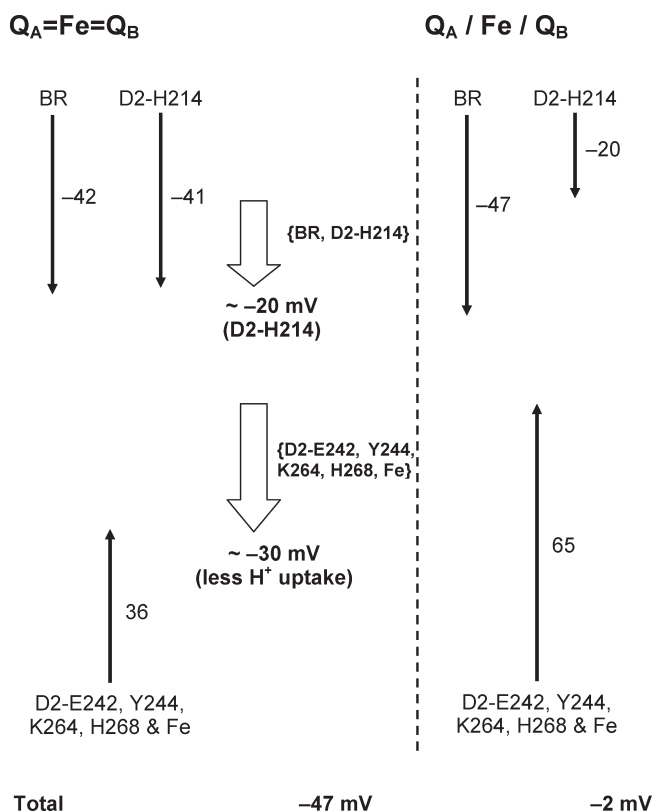


Figure 3. Summary of the key components that differentiate the $\Delta E_m(Q_A)_{PQ \rightarrow BR}$ up- and downshift in the conjugated Q_A –Fe– Q_B and nonconjugated $Q_A/Fe/Q_B$ systems. The thin arrow indicates the E_m shifts due to each component. The thick empty arrows indicate the net E_m shift ($\{BR, D2-His214\}$ or $\{D2-Glu242, Tyr244, Lys264, His268, Fe\}$) for the Q_A –Fe– Q_B system relative to the $Q_A/Fe/Q_B$ system.

system, the $\Delta E_m(Q_A)_{PQ \rightarrow BR}$ downshift of 95 mV due to the residues listed in Table 1a is only partially offset by those listed in Table 1b (40 mV), resulting in the total $\Delta E_m(Q_A)_{PQ \rightarrow BR}$ downshift of ~ 50 mV. Thus, in addition to the conjugation effect pronounced at D2-His214, the difference in the compensation for the $\Delta E_m(Q_A)_{PQ \rightarrow BR}$ downshift due to protein components is also a main reason why the experimentally measured value of -45 mV⁶ can be reproduced only in the conjugated Q_A –Fe– Q_B system [$\Delta E_m(Q_A)_{PQ \rightarrow BR} = -55$ mV] and not in the nonconjugated $Q_A/Fe/Q_B$ system [$\Delta E_m(Q_A)_{PQ \rightarrow BR} = -13$ mV] (Figure 3).

Protonation State Changes in the D–de Loop. In previous studies on the non-heme Fe,⁵ significant changes in the protonation states of residues located in the D–de loop were observed in response to changes in the redox state of the non-

Table 2. Residues That Alter the Protonation State for the PQ- and BR-Bound PSII in H^+ Units^a

Q_B site	Q_A –Fe– Q_B			$Q_A/Fe/Q_B$		
	PQ	BR	difference	PQ	BR	difference
D2-Arg139	0.66	0.80	–0.14	0.67	0.78	–0.12
D2-Tyr141	0.85	0.92	–0.07	0.84	0.92	–0.07
D2-Glu242	0.46	0.52	–0.07	0.58	0.43	0.14
D2-Tyr244	0.95	1.00	–0.05	0.79	0.99	–0.20
D2-Lys264	0.91	1.00	–0.09	0.87	0.98	–0.11

^a Protonation states were calculated with Q_A 50% reduced. Fully protonated and deprotonated states were defined as protonation states 1.0 H^+ and 0.0 H^+ , respectively.

heme Fe or quinones. Additionally, it was concluded that five Glu residues in the D–de loops and six basic residues near the non-heme Fe are responsible for the experimentally measured pH dependence of $E_m(Fe)$,^{34–36} implying the existence of a network of residues serving as an internal proton reservoir,⁵ which may correspond to a cluster of acidic residues in the bacterial reaction centers near quinones.³⁷ Indeed, D2-Tyr244, D2-Lys264, and D2-Glu242 listed in Table 1b are residues located in either the D–de loop or the neighborhood of the non-heme Fe (Figure 1).

In this study, we found that the protonation states of residues D2-Tyr244, D2-Lys264, and D2-Glu242 that upshift $\Delta E_m(Q_A)_{PQ \rightarrow BR}$ (listed in Table 1b) are notably different in the Q_A –Fe–PQ and $Q_A/Fe/PQ$ systems (Table 2). In particular, the protonation state difference between the PQ- and BR-bound PSII is larger in the $Q_A/Fe/Q_B$ system than in the Q_A –Fe– Q_B system. Apparently, the more protonated state in the $Q_A/Fe/Q_B$ system compensates for the $\Delta E_m(Q_A)_{PQ \rightarrow BR}$ downshift due to the groups listed in Table 1a because the proton uptake events of the titratable residues in the $Q_A/Fe/PQ$ system with regard to the $Q_A/Fe/BR$ system lead to an increase in the residue net charge, resulting in the $\Delta E_m(Q_A)_{PQ \rightarrow BR}$ upshift. Thus, the $\Delta E_m(Q_A)_{PQ \rightarrow BR}$ value in the $Q_A/Fe/PQ$ system is almost equal to the $\Delta E_m(Q_A)_{PQ \rightarrow BR}$ value in the $Q_A/Fe/BR$ system, resulting in a $\Delta E_m(Q_A)_{PQ \rightarrow BR}$ value of only -13 mV. Hence, the influence of the net charge decrease of -1 on $\Delta E_m(Q_A)_{PQ \rightarrow BR}$ due to the replacement of PQ with deprotonated BR is offset by the proton uptake events in the D–de loop (Figure 3).

On the other hand, in the conjugated Q_A –Fe– Q_B system, D2-Tyr244 and D2-Lys264 do not significantly change their protonation states in response to the replacement of PQ with BR (Table 2). Thus, the influence of the proton uptake events of the two residues on $\Delta E_m(Q_A)_{PQ \rightarrow BR}$ is considerably small in the Q_A –Fe– Q_B system. This is because the atomic partial charges

are more moderately distributed over the large Q_A –Fe– Q_B complex than the Q_A /Fe/ Q_B system. Because of the charge delocalization effect in the Q_A –Fe– Q_B system, the negative charge originally located in the Q_B region (–1.0 on BR) is decreased to –0.76 (Table S1 of the Supporting Information), and in turn, the net charge on the Fe region is decreased by 0.33. In doing so, replacement of PQ with BR in the Q_A –Fe– Q_B system could suppress external counteractions, protonation state changes of the titratable residues. Therefore, the influence of the BR negative charge is effectively propagated to the Q_A region without being shielded by the residue proton uptake events.

To explain the experimentally measured value of –45 mV,⁶ we can conclude that the existence of the internal long-distance charge delocalization effect over the Q_A –Fe– Q_B network plays an important role in suppressing external counteraction, a residue protonation pattern change that would otherwise negate the influence on $\Delta E_m(Q_A)_{PQ \rightarrow BR}$ due to the replacement of PQ with BR.

CONCLUSION

An experimentally measured value of approximately –45 mV⁶ can be reproduced only when Q_A , the non-heme Fe, and the Q_B site are considered as a conjugated supramolecular Q_A –Fe– Q_B system, yielding a $\Delta E_m(Q_A)_{PQ \rightarrow BR}$ of –55 mV. In both conjugated Q_A –Fe– Q_B and nonconjugated Q_A /Fe/ Q_B systems, BR downshifts $\Delta E_m(Q_A)_{PQ \rightarrow BR}$ almost equally by 42–47 mV (Table 1a). However, the influence of the Q_A H-bond donor D2-His214 on $\Delta E_m(Q_A)_{PQ \rightarrow BR}$ is 2 times larger in the Q_A –Fe– Q_B system (–41 mV) than in the Q_A /Fe/ Q_B system (–20 mV) as a result of the charge redistribution due to the conjugation.

From the analysis of the calculated $\Delta E_m(Q_A)_{PQ \rightarrow BR}$ of –55 mV, the character of the molecule at the Q_B binding site can be propagated to Q_A via the non-heme Fe and two ligands, D1-His215 and D2-His214, due to the conjugation effect of the Q_A –Fe– Q_B system. In particular, the Q_B character strongly appears in D2-His214 (Table 1), the H-bond donor for Q_A , indicating that D2-His214 is the residue that controls $E_m(Q_A)$. This control mode, originally proposed from studies of the bacterial photosynthetic reaction centers^{28–33} and recently confirmed by FTIR studies on PSII,¹² is quite effective in facilitating a long-distance interaction with Q_A from the Q_B side. Charge delocalization due to the conjugation effect leads to an internal moderate charge distribution over the Q_A –Fe– Q_B system (including the H-bond strength change between D1-His214 and Q_A), preventing external protonation state changes of the titratable residues that would otherwise neutralize the influence of the induced net charge change in the replacement of PQ with BR (Figure 3).

The charge delocalization effect propagates the Q_B character to $E_m(Q_A)$ by directly affecting D2-His214 (donates an H-bond to Q_A), without causing counteraction such as proton uptake events of the titratable residues near the non-heme Fe region.

ASSOCIATED CONTENT

S Supporting Information. Atomic coordinates of the PQ- and BR-bound PSII structures and atomic partial charges for the Q_A –Fe– Q_B system (Q_B = BR or PQ) and the non-heme Fe (for the Q_A /Fe/ Q_B system). This material is available free of charge via the Internet at <http://pubs.acs.org>.

AUTHOR INFORMATION

Corresponding Author

*Address: 202 Building E, Career-Path Promotion Unit for Young Life Scientists, Graduate School of Medicine, Kyoto University, Yoshida-Konoe-cho, Sakyo-ku, Kyoto 606-8501, Japan. Telephone: +81-75-753-9286. Fax: +81-75-753-9286. E-mail: hiro@cp.kyoto-u.ac.jp.

Funding Sources

This work was supported by the JST PRESTO program, Grants-in-Aid for Science Research from the Ministry of Education, Science, Sport and Culture of Japan (21770163 to H.I. and 21108506 and 21370063 to T.N.), the Special Coordination Fund for Promoting Science and Technology of MEXT, and the Takeda Science Foundation.

ACKNOWLEDGMENT

We thank Dr. Miwa Sugiura for useful discussions.

ABBREVIATIONS

BR, bromoxynil in the deprotonated form; BR- and PQ-bound PSII, PSII structure in which BR and PQ are at the Q_B binding site, respectively; Chl_{D1}, accessory chlorophyll on the D1 side; DCMU, 3-(3,4-dichlorophenyl)-1,1-dimethylurea; $\Delta E_m(Q_A)_{PQ \rightarrow BR}$, [$E_m(Q_A)$ in BR-bound PSII] – [$E_m(Q_A)$ in PQ-bound PSII]; D–de loop, hydrophilic loop in D1 and D2 that connects transmembrane helix D with parallel helix de; E_m , (midpoint) redox potential; FTIR, Fourier transform infrared; LPB, linearized Poisson–Boltzmann; MnCa cluster, oxygen-evolving complex; non-heme Fe, Fe complex ligated by four His residues and one bicarbonate; PQ, plastoquinone; PSII, photosystem II; Q_B , Q_B binding site where either PQ or BR is situated; Q_A –Fe– Q_B , conjugated supramolecular system in which DFT calculations were performed for the entire Q_A , the non-heme Fe, and Q_B ; Q_A /Fe/ Q_B , nonconjugated system in which DFT calculations were performed separately for Q_A , the non-heme Fe, and Q_B molecules

REFERENCES

- (1) Prokhorenko, V. I., and Holzwarth, A. R. (2000) Primary process and structure of the photosystem II reaction center: A photon echo study. *J. Phys. Chem. B* 104, 11563–11578.
- (2) Diner, B. A., and Rappaport, F. (2002) Structure dynamics, and energetics of the primary photochemistry of photosystem II of oxygenic photosynthesis. *Annu. Rev. Plant Biol.* 53, 551–580.
- (3) Renger, G., and Renger, T. (2008) Photosystem II: The machinery of photosynthetic water splitting. *Photosynth. Res.* 98, 53–80.
- (4) Petrouleas, V., and Crofts, A. R. (2005) The quinone iron acceptor complex. In *Photosystem II: The Light-Driven Water: Plastoquinone Oxidoreductase* (Wydrzynski, T., and Satoh, K., Eds.) pp 177–206, Springer, Dordrecht, The Netherlands.
- (5) Ishikita, H., and Knapp, E.-W. (2005) Oxidation of the non-heme iron complex in photosystem II. *Biochemistry* 44, 14772–14783.
- (6) Krieger-Liszka, A., and Rutherford, A. W. (1998) Influence of herbicide binding on the redox potential of the quinone acceptor in photosystem II: Relevance to photodamage and phytotoxicity. *Biochemistry* 37, 17339–17344.
- (7) Johnson, G. N., Rutherford, A. W., and Krieger, A. (1995) A change in the midpoint potential of the quinone Q_A in Photosystem II associated with photoactivation of oxygen evolution. *Biochim. Biophys. Acta* 1229, 202–207.

- (8) Ishikita, H., and Knapp, E.-W. (2005) Control of quinone redox potentials in photosystem II: Electron transfer and photoprotection. *J. Am. Chem. Soc.* 127, 14714–14720.
- (9) Gunner, M. R., Robertson, D. E., and Dutton, P. L. (1986) Kinetic studies on the reaction center protein from *Rhodospseudomonas sphaeroides*: The temperature and free energy dependence of electron transfer between various quinones in the Q_A site and the oxidized bacteriochlorophyll dimer. *J. Phys. Chem.* 90, 3783–3795.
- (10) Shopes, R. J., and Wraight, C. A. (1987) Charge recombination from the $P^+Q_A^-$ state in reaction centers from *Rhodospseudomonas viridis*. *Biochim. Biophys. Acta* 893, 409–425.
- (11) Rappaport, F., Guergova-Kuras, M., Nixon, P. J., Diner, B. A., and Lavergne, J. (2002) Kinetics and pathways of charge recombination in photosystem II. *Biochemistry* 41, 8518–8527.
- (12) Takano, A., Takahashi, R., Suzuki, H., and Noguchi, T. (2008) Herbicide effect on the hydrogen-bonding interaction of the primary quinone electron acceptor Q_A in photosystem II as studied by Fourier transform infrared spectroscopy. *Photosynth. Res.* 98, 159–167.
- (13) Takahashi, R., Hasegawa, K., Takano, A., and Noguchi, T. (2010) Structures and binding sites of phenolic herbicides in the Q_B pocket of photosystem II. *Biochemistry* 49, 5445–5454.
- (14) Guskov, A., Kern, J., Gabdulkhakov, A., Broser, M., Zouni, A., and Saenger, W. (2009) Cyanobacterial photosystem II at 2.9-Å resolution and the role of quinones, lipids, channels and chloride. *Nat. Struct. Mol. Biol.* 16, 334–342.
- (15) Ogawa, T., and Nakano, T. (2010) Extended universal force field (XUFF): Theory and applications. *Chem-Bio Inf. J.* 10, 111–133.
- (16) BioStation, version 3.2 (2009) AdvanceSoft Corp., Tokyo.
- (17) AutoDock 4.2 and AutoDockTools (2009) The Scripps Research Institute, La Jolla, CA.
- (18) Brooks, B. R., Bruccoleri, R. E., Olafson, B. D., States, D. J., Swaminathan, S., and Karplus, M. (1983) CHARMM: A program for macromolecular energy minimization and dynamics calculations. *J. Comput. Chem.* 4, 187–217.
- (19) MacKerell, A. D., Jr., Bashford, D., Bellott, R. L., Dunbrack, R. L., Jr., Evanseck, J. D., Field, M. J., Fischer, S., Gao, J., Guo, H., Ha, S., Joseph-McCarthy, D., Kuchnir, L., Kuczera, K., Lau, F. T. K., Mattos, C., Michnick, S., Ngo, T., Nguyen, D. T., Prodhom, B., Reiher, W. E., III, Roux, B., Schlenkrich, M., Smith, J. C., Stote, R., Straub, J., Watanabe, M., Wiorkiewicz-Kuczera, J., Yin, D., and Karplus, M. (1998) All-atom empirical potential for molecular modeling and dynamics studies of proteins. *J. Phys. Chem. B* 102, 3586–3616.
- (20) Rabenstein, B., Ullmann, G. M., and Knapp, E.-W. (1998) Calculation of protonation patterns in proteins with structural relaxation and molecular ensembles: Application to the photosynthetic reaction center. *Eur. Biophys. J.* 27, 626–637.
- (21) Ishikita, H., Saenger, W., Biesiadka, J., Loll, B., and Knapp, E.-W. (2006) How photosynthetic reaction centers control oxidation power in chlorophyll pairs P680, P700 and P870. *Proc. Natl. Acad. Sci. U.S.A.* 103, 9855–9860.
- (22) Bayly, C. I., Cieplak, P., Cornell, W. D., and Kollman, P. A. (1993) A well-behaved electrostatic potential based method using charge restraints for deriving atomic charges: The RESP model. *J. Phys. Chem.* 97, 10269–10280.
- (23) Jaguar4.2 (2000) Schrödinger, Inc., Portland, OR.
- (24) Bashford, D., and Karplus, M. (1990) pK_a 's of ionizable groups in proteins: Atomic detail from a continuum electrostatic model. *Biochemistry* 29, 10219–10225.
- (25) Rabenstein, B., and Knapp, E. W. (2001) Calculated pH-dependent population and protonation of carbon-monooxy-myoglobin conformers. *Biophys. J.* 80, 1141–1150.
- (26) Ishikita, H., and Knapp, E.-W. (2004) Variation of Ser-L223 hydrogen bonding with the Q_B redox state in reaction centers from *Rhodobacter sphaeroides*. *J. Am. Chem. Soc.* 126, 8059–8064.
- (27) Zhu, Z., and Gunner, M. R. (2005) Energetics of quinone-dependent electron and proton transfers in *Rhodobacter sphaeroides* photosynthetic reaction centers. *Biochemistry* 44, 82–96.
- (28) Maroti, P., Hanson, D. K., Schiffer, M., and Sebban, P. (1995) Long-range electrostatic interaction in the bacterial photosynthetic reaction centre. *Nat. Struct. Biol.* 2, 1057–1059.
- (29) Baciou, L., Sinning, I., and Sebban, P. (1991) Study of Q_B^- stabilization in herbicide-resistant mutants from the purple bacterium *Rhodospseudomonas viridis*. *Biochemistry* 30, 9110–9116.
- (30) Baciou, L., and Sebban, P. (1995) Heterogeneity of the quinone electron acceptor system in bacterial reaction centers. *Photochem. Photobiol.* 62, 271–278.
- (31) Fufezan, C., Drepper, F., Juhnke, H. D., Lancaster, C. R. D., Un, S., Rutherford, A. W., and Krieger-Liszskay, A. (2005) Herbicide-induced changes in charge recombination and redox potential of Q_A in the T4 mutant of *Blastochloris viridis*. *Biochemistry* 44, 5931–5939.
- (32) Spitz, J. A., Derrien, V., Baciou, L., and Sebban, P. (2005) Specific triazine resistance in bacterial reaction centers induced by a single mutation in the Q_A protein pocket. *Biochemistry* 44, 1338–1343.
- (33) Cheap, H., Tandori, J., Derrien, V., Benoit, M., de Oliveira, P., Koepke, J., Lavergne, J., Maroti, P., and Sebban, P. (2007) Evidence for delocalized anticooperative flash induced proton binding as revealed by mutants at the M266His iron ligand in bacterial reaction centers. *Biochemistry* 46, 4510–4521.
- (34) Bowes, J. M., Crofts, A. R., and Itoh, S. (1979) A high potential acceptor for Photosystem II. *Biochim. Biophys. Acta* 547, 320–335.
- (35) Wraight, C. A. (1985) Modulation of herbicide-binding by the redox state of Q_{400} , an endogenous component of photosystem II. *Biochim. Biophys. Acta* 809, 320–330.
- (36) Petrouleas, V., and Diner, B. A. (1986) Identification of Q_{400} , a high-potential electron acceptor of Photosystem II, with the iron of the quinone-iron acceptor complex. *Biochim. Biophys. Acta* 849, 264–275.
- (37) Abresch, E. C., Paddock, M. L., Stowell, M. H. B., McPhillips, T. M., Axelrod, H. L., Soltis, S. M., Rees, D. C., Okamura, M. Y., and Feher, G. (1998) Identification of proton transfer pathways in the X-ray crystal structure of the bacterial reaction center from *Rhodobacter sphaeroides*. *Photosynth. Res.* 55, 119–125.